RSC Advances

PAPER

View Article Online
View Journal | View Issue

Cite this: *RSC Adv.*, 2024, **14**, 30673

Insight into the synthesis, structure affirmation and catalytic efficiency of divalent and trivalent metal chelates of mandelic acid hydrazone derivative†

Hoda A. El-Ghamry, *[a] Mohamed Gaber,[a] Fatmah M. Alkhatib,[b] Hossa F. Al Shareef,[b] Khadiga M. Takroni[b] and Shaimaa K. Fathalla[c]

The current work reports the synthesis of Cr(III), Mn(II), Co(II), Ni(II) and Cu(II) chelates of the Schiff base ligand named hydroxy-phenyl-acetic acid (2-hydroxy-naphthalen-1-ylmethylene)-hydrazide with multi-chelation centre toward metal ions. The spectral tools, ^{1}H-NMR, FTIR, mass, UV-vis spectra, and the analytical elemental and thermal analysis, in addition to magnetic moment and conductivity measurements all combined have been applied to conclude the structure and geometry of the synthesized metal complexes. The formed metal chelates have been assured to be formed with the molar compositions of 1 L : 1 M for **PANH-Cr**, **PANH-Mn**, **PANH-Co**, **PANH-Ni** and 2 L : 1 M for **PANH-Cu**. All the complexes have been confirmed to be non-electrolytic except the **PANH-Mn** and **PANH-Ni** which are 1 : 1 electrolytes. FTIR spectral analysis assured the ligand to act as mono basic bi or tridentate ligand leading to the formation of octahedral complexes with all metals except Cu(II) complex which assured to has square planar structure. Except **PANH-Cr**, all the synthesized metal chelates exhibited phenoxazinone synthase like efficacy with varying activity with dramatically high activity for **PANH-Mn** complex with TOF number of 169.89 h^{-1}.

Received 9th August 2024
Accepted 18th September 2024

DOI: 10.1039/d4ra05769d

rsc.li/rsc-advances

1. Introduction

Hydrazones are considered flexible ligands that are classified as azomethine compounds, having the structure $R_2C{=}NNR_2$. They are distinguished from other members of this class, such as oximes, imines, and others, by the presence of linked nitrogen atoms.[1]

Hydrazone-based ligands have gained interest due to their numerous coordination characteristics and capacity to coordinate in both protonated and deprotonated forms.[2,3] A dominant contribution in the advancement of coordination chemistry was achieved by hydrazone ligands formed by the condensation reaction of *o*-hydroxyaldehydes and ketones with hydrazides due to the formed conceivable poly-cleating ligands that pass amide, azomethine and phenol functionalities and provide a variety of bonding options to metal centres in metal chelates.[4] Benzoylhydrazones of salicylaldehyde,[5] 2-hydroxy-1-naphthaldehyde[6] and their analogies compounds[7,8] are considered the most important hydrazone ligands since this structure building provide a class of ligands with bi-or tridentate cavity coordinating to the metal centres through the carbonyl oxygen, azomethine nitrogen and hydroxyl oxygen resulting in the formation of five and/or six membered chelate ring surrounding the metal centre. Condensation of 2-hydroxy-1-naphthaldehyde with mandelic acid hydrazide resulting in the formation of analogies ligand structure.

The great importance of hydrazone compounds and their metal chelates steam from their wide range of applications since they are applied in biological system as antimicrobial, antibiotic, antimalarial and antitumor[9–12] beside their uses in analytical,[13] catalytic[14–16] applications and also as molecular sensors[17] and luminescent probes.[18]

Among the transition elements, Mn element is considered a significant element for human healthiness, metabolism, antioxidant system and fundamental in photosystem for O_2 evolution.[19–22] Recently, great attention has been allocated for the design and synthesis of Mn coordination compounds due to their efficiently catalytic performance[23–26] specifically with Schiff base ligands incorporating N and O atoms. The reason is that in such complexes the Mn(II) centers are subjected to aerial oxidation to form complexes in which Mn ion is oxidized to higher oxidation states (*i.e.* Mn(III) and/or Mn(IV)).[27] Among the important catalytic reaction for Mn complexes is bio-mimicking oxidase (*e.g.* catecholase and phenoxazinone synthase) and oxygenase (*e.g.* epoxidation) reactions.[27–30]

[a]*Chemistry Department, Faculty of Science, Tanta University, Tanta, Egypt. E-mail: hoda.elghamri@science.tanta.edu.eg*

[b]*Chemistry Department, Faculty of Applied Science, Umm Al-Qura University, Makkah, Saudi Arabia*

[c]*Chemistry Department, Faculty of Science, Taif University, Taif, Saudi Arabia*

† Electronic supplementary information (ESI) available. See DOI: https://doi.org/10.1039/d4ra05769d

Phenoxazinone synthase is one of the enzymes whose behavior and effects have been experimentally and widely mimicked experimentally. This enzyme is called poly nuclear copper oxidase. This enzyme acts as a catalyst for the oxidative condensation of *o*-aminophenol and its derivatives to phenoxazinone chromophore and is found naturally in the bacteria *Streptomyces* antibioticus. This phenoxazinone chromophore is used therapeutically to treat Wilm's tumor curing, gestational choriocarcinoma, and other tumor types. Its function is to stop DNA intercalation from synthesizing RNA based on DNA in these tumor kinds.[31] The major condition for a metal chelate to be as promising as phenoxazinone synthase is the availability of labile positions on the metal centers. Metal complexes incorporating other metals such as Cu(II), Co(II) and Ru(III) are also reported to catalyse such reactions.[31–35]

All the previous facts motivated us to design and prepare a number of metal complexes of the hydrazone ligand named hydroxy-phenyl-acetic acid (2-hydroxy-naphthalen-1-ylmethylene)-hydrazide. Structure assertion of the synthesized metal ion chelates (Cr(III), Mn(II), Co(II), Ni(II) and Cu(II) chelates) were performed using the analytical and spectral methods. The interested complexes have been tested and evaluated for their catalytic activity as phenoxazinone synthase.

2. Experimental

2.1. Preparation of the Schiff base ligand (PANH)

The target Schiff base has been synthesised as previously reported.[8] 0.01 mol of 2-hydroxy-1-naphthaldehyde and mandelic acid hydrazide (1.72 g and 1.66 g, respectively) were separately solubilized in the least sufficient amount of hot MeOH followed by slow addition of one solution to the other. The final solution was allowed for reflux at 60 °C for 4 h within which yellowish crystalline needles have been appeared. The hot reaction solution was filtered to separate the formed compound which rinsed several times using hot methanol and eventually with ether. The product was kept drying in vacuum desiccator (Fig. 1). Purity of the ligand has been assured by ^{1}H-NMR, FTIR, mass and elemental analysis.

^{1}H-NMR (600 MHz, DMSO-d$_6$, δ, ppm): δ: 3.81 (s, 1H, CH–O**H**), 5.17 (s, 1H, C**H**–OH), 6.65 (s, br, 1H, NH), 7.16–7.9 (d, m, 11H, Ar–H), 8.17 (s, 1H, CH=N), 9.51 (s, 1H, phenolic OH).

2.2. Synthesis of metal chelates

The above mentioned multidentate ligand (*i.e.* **PANH**) has been used for the synthesis of the Cr(III), Mn(II), Co(II), Ni(II) and Cu(II) chelates through dissolving 0.001 mol of each of $Cr(CH_3COO)_3$ (0.232 g) $MnCl_2 \cdot 4H_2O$ (0.197 g), $CoCl_2 \cdot 6H_2O$ (0.237 g), $NiCl_2 \cdot 6H_2O$ (0.237 g) and $Cu(CH_3COO) \cdot H_2O$ (0.199 g) in the least sufficient quantity of hot MeOH and added separately to a heated methanolic solution that included 0.32 g (0.001 mol of **PANH**). The resultant mixtures were refluxed for eight hours at boiling temperature, during which time colorful compounds developed. After being filtered out, the solid products were repeatedly washed with hot methanol and then with ether. The product was maintained in a vacuum desiccator for drying out.

2.3. Measurements instrumentation and OAP catalytic oxidation

The Sigma-Aldrich company is the supplier for all of the analytical grade reagents used in the current study, which were used exactly as they were given. Information regarding the tools and techniques used for structure assertion and implementation is provided from the previously reported study.[31] Using *o*-aminophenol as the substrate, the methods and strategies employed to assign the complexes under investigation's phenoxazinone synthase-like activity are generally as previously mentioned[34] and as described in details in the ESI file.†

3. Results and discussion

3.1. ^{1}H NMR spectra of PANH ligand

Fig. 2 represents the ^{1}H-NMR spectrum of **PANH** ligand measured in DMSO-d$_6$ using the internal standard tetramethylsilane (TMS). The signal appearing at 9.51 ppm has been appointed to the phenolic proton whereas the one appearing at 8.17 ppm is assigned to the azomethine proton. The broad signal that appeared at 6.6 ppm has been attributed to the NH proton.[36]

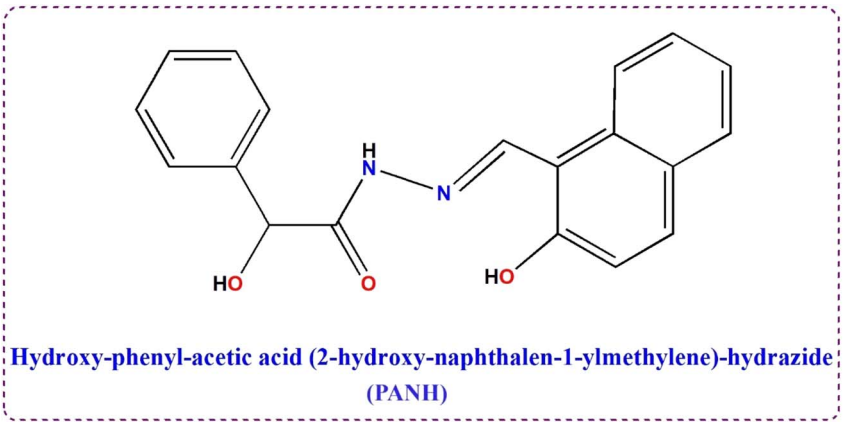

Fig. 1 Structure of the ligand PANH with the IUPAC name.

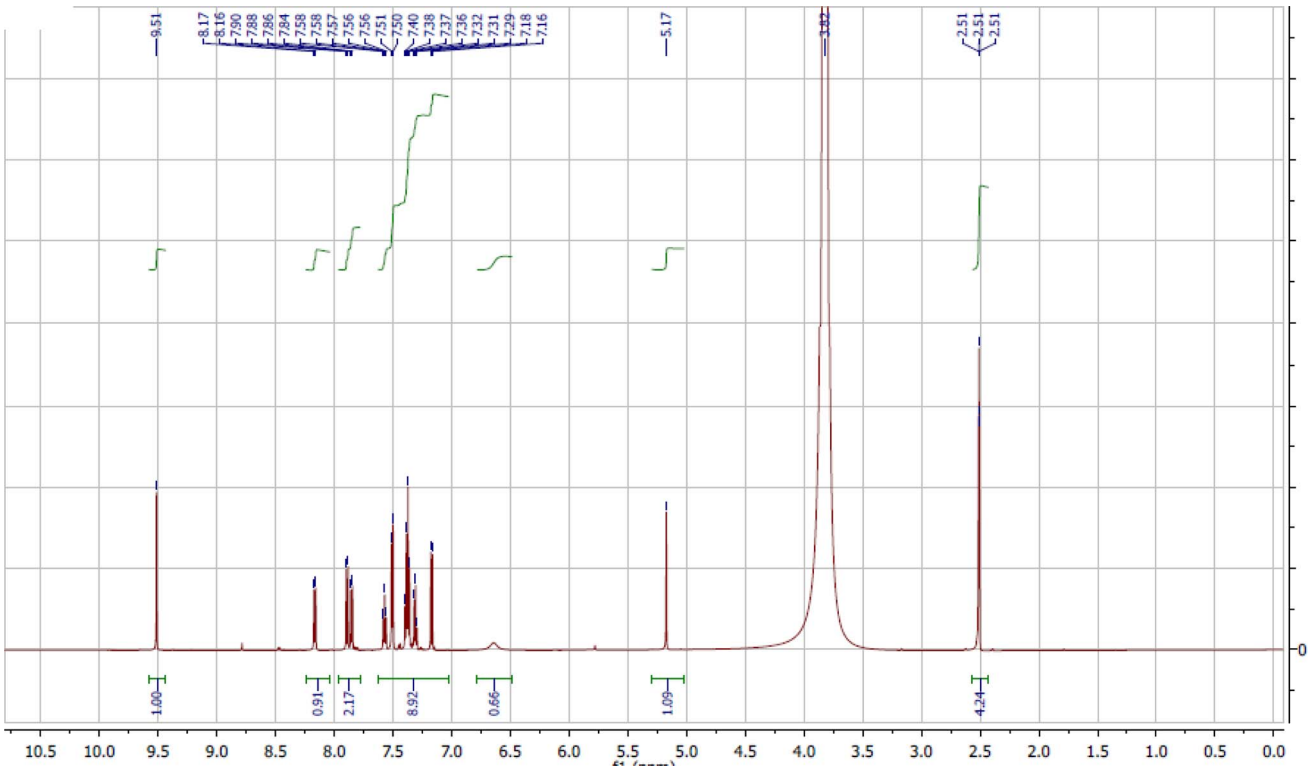

Fig. 2 ^{1}H-NMR spectrum of the ligand **PANH** in DMSO-d_6 solvent.

Aromatic protons of the phenyl and naphthyl rings featured as doublet and multiple signals inside 7.9–7.16 ppm range. The aliphatic CH and OH protons appeared at 5.17 and 3.81 ppm, respectively.[37,38] The OH proton signal at 3.81 ppm is overlapped with the solvent signal as it is appearing in the same range.

3.2. Complexes composition and conductivity

As concluded from the results of the contained elements percent, the isolated metal chelates have been formed in the molar composition 1 L : 1 M for **PANH-Cr**, **PANH-Mn**, **PANH-Co**, **PANH-Ni**. For the Cu(II) complex, **PANH-Cu**, although it has been synthesized in the molar ratio 1 L : 1 M, the isolated complex formed in 2 L : 1 M ratio. The molecular formulas of all complexes were concluded to be $[Cr(PANH)(AOc)_2H_2O]\cdot H_2O$, $[Mn(PANH)(H_2O)_3]\cdot Cl\cdot 2H_2O$, $[Co(PANH)Cl(H_2O)_2]\cdot 3H_2O$, $[Ni(PANH)(H_2O)_3]\cdot Cl\cdot 2H_2O$ and $[Cu(PANH)_2]$; Table 1. The solubility test of the highly stable complexes indicated that all complexes have no solubility in all non-polar solvents, partially soluble in MeOH and EtOH and extremely soluble in MeCN, DMSO and DMF. The molar conductivity values as measured

Table 1 Elemental analysis and physical properties of the complexes under investigation

Comp. symbol	Ligand/complex (molecular formula; *M*. wt)	Colour (m.p. °C)	Elemental analysis[b] % C	% H	% N	% M	Λ_m
PANH	($C_{19}H_{16}N_2O_3$; 320.34)	Yellow (242)	71.24 (71.32)	5.03 (5.14)	8.47 (8.53)	—	—
PANH-Cr	$[Cr(PANH)(AOc)_2H_2O]\cdot H_2O$ ($C_{23}H_{25}CrN_2O_9$; 525.45)	Yellowish green (294)	52.57 (52.69)	4.80 (4.68)	5.33 (5.21)	9.90 (9.74)	17.2
PANH-Mn	$[Mn(PANH)(H_2O)_3]\cdot Cl\cdot 2H_2O$ ($C_{19}H_{25}ClMnN_2O_8$, 499.80)	Brown (275)[a]	45.66 (45.76)	5.04 (5.24)	5.60 (5.73)	10.99 (11.77)	69.5
PANH-Co	$[Co(PANH)Cl(H_2O)_2]\cdot 3H_2O$ ($C_{19}H_{23}ClCoN_2O_7$; 485.78)	Brown (252)[a]	46.98 (47.22)	4.77 (4.81)	5.77 (5.92)	12.13 (12.93)	18.6
PANH-Ni	$[Ni(PANH)(H_2O)_3]\cdot Cl\cdot 2H_2O$ ($C_{19}H_{25}ClNiN_2O_8$; 503.56)	Dark yellow (>300)	45.32 (45.45)	5.00 (5.23)	5.56 (5.71)	11.66 (11.40)	71.4
PANH-Cu	$[Cu(PANH)_2]$ ($C_{38}H_{30}CuN_4O_6$; 702.21)	Olive green (265)[a]	65.00 (65.17)	4.31 (4.39)	7.98 (8.26)	9.05 (9.49)	15.7

[a] Decomposition temperature. [b] Calculated (Found).

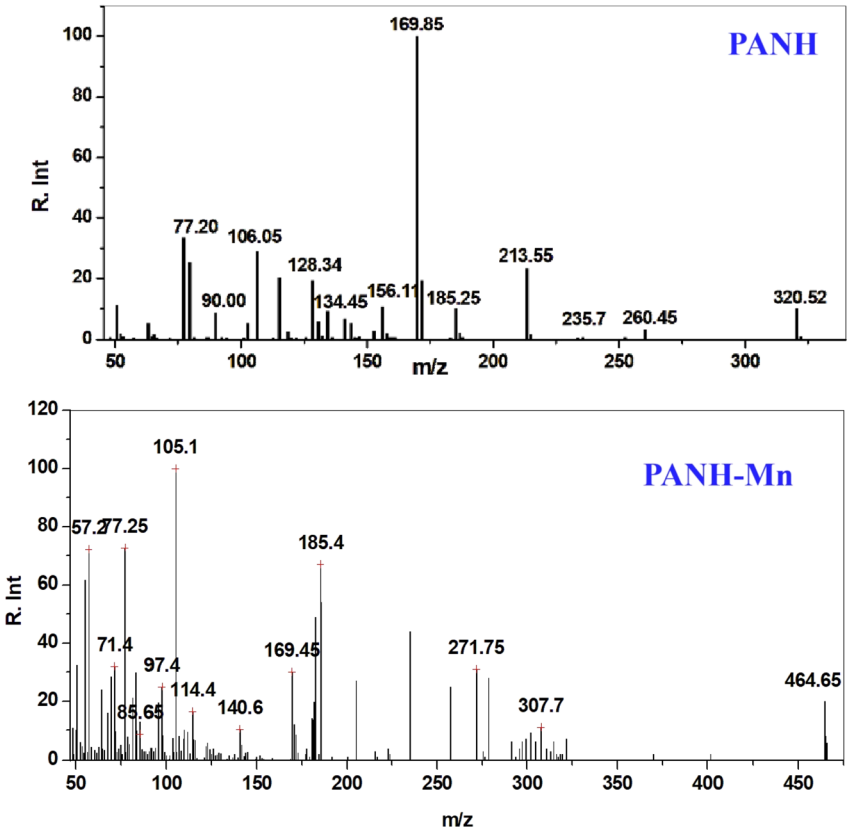

Fig. 3 Mass spectra of PANH ligand and PANH-Mn chelate.

from 10^{-3} M solution of each compound dissolved in DMSO were found to be 17.2, 69.5, 18.6, 71.4 and 15.7 Ω^{-1} cm^2 mol^{-1} for **PANH-Cr**, **PANH-Mn**, **PANH-Co**, **PANH-Ni** and **PANH-Cu**, successively, which is in good matching with the non-electrolytic features of **PANH-Cr**, **PANH-Co**, and **PANH-Cu** complexes and 1 : 1 electrolyte for and **PANH-Mn** and **PANH-Ni** as compared by reported compounds.[39,40]

3.3 EI-mass spectra

The prospected molecular weights of the ligand, **PANH**, and its chelates, **PANH-Cr**, **PANH-Mn**, **PANH-Co**, **PANH-Ni** and **PANH-Cu**, have been assured through comparison of the mass spectral results. The molecular weight of the ligand and **PANH-Mn** complex were found to be 320.52 and 464.65 matching with the theoretical molecular weight of the ligand (*i.e.* 320.34) and M − 1 for **PANH-Mn** (without hydration water molecules); Fig. 3. The mass spectra of complexes **PANH-Cr**, **PANH-Co**, **PANH-Ni** and **PANH-Cu** (Fig. S1–S4†) gave the molecular ion peaks at 509.25 (M + 2 − 2H_2O), 449.92 (M − 2H_2O), 466.58 (M − 1 − 2H_2O) and 705.62 (M + 3), respectively, which is in large agreement with the concluded molecular weights.

3.4. IR spectra and mode of bonding

The coordinating function groups in the ligand to the metal centers can be identified by comparing the FTIR spectra of the metal complexes with those of the free Schiff base, **PANH**. Changes in position and/or intensity of spectral bands are common in coordinating function groups. It's also possible for some bands to disappear during chelation. The most important infrared bands of **PANH** and its complexes are shown in Table 2, along with their respective assignments, the spectra are shown in Fig. 4, 5 & S5.†

The bands in the spectra of **PANH** that appeared at 3353 and 3052 cm^{-1} were assigned to the stretching vibrations of the OH and NH groups, respectively, according to an analysis of the results shown in Table 2. While the band at 1622 cm^{-1} was linked to ν(C=N) groups, the band at 1675 cm^{-1} was related to the stretching vibration of C=O. Two bands have been assigned

Table 2 Assignment of the IR bands of PANH and its complexes

Comp.	ν_{OH}	ν_{NH}	$\nu_{C=O}$	$\nu_{C=N}$	ν_{C-O}[a,b]	ν_{C-O}	ν_{M-N}
PANH	3353	3052	1675	1622	1285 1221	—	—
PANH-Cr	3415	3054	1649	1613	1250 1220	536	448
PANH-Mn	3422	3056	1649	1617	1248 1220	542	443
PANH-Co	3418	3052	1652(sh)	1617	1249 1220	545	463
PANH-Ni	3414	3060	1656	1617	1247 1192	529	460
PANH-Cu	3416	3073	1643(sh)	1619	1284 1193	528	—

[a] Phenolic. [b] 2° alcohol.

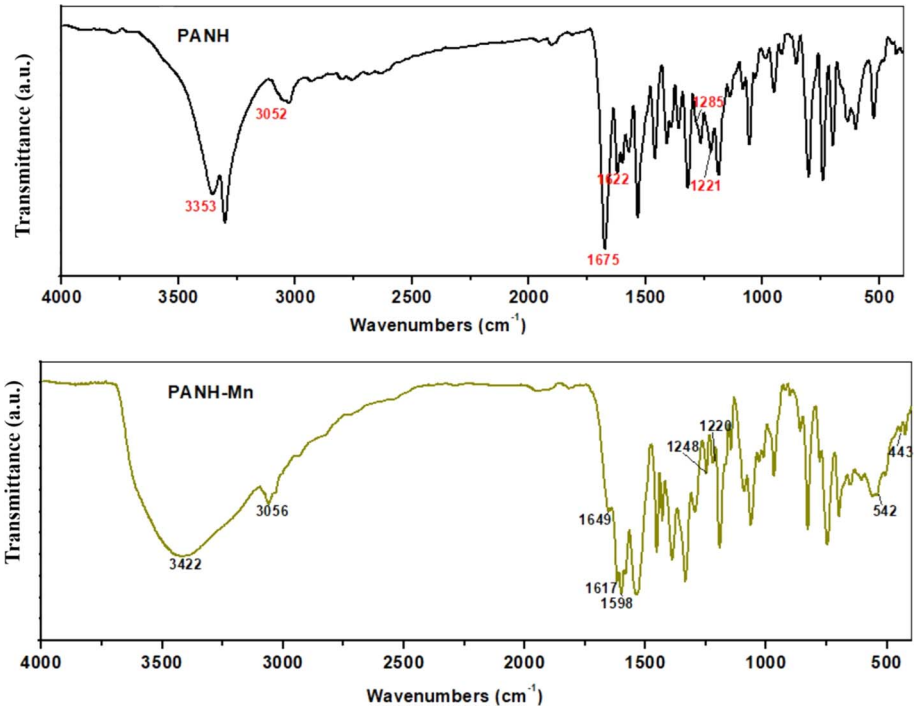

Fig. 4 IR spectra of **PANH** in comparison & **PANH-Mn** complex.

to phenolic and secondary alcoholic C–O stretching at 1285 and 1221 cm^{-1}, respectively.[41,42]

In the spectra of metal complexes **PANH-Cr**, **PANH-Mn**, **PANH-Co** and **PANH-Ni**, the three bands corresponding to the ν(C=O), ν(C=N) and ν(C–$O_{phenolic}$) appeared within the ranges 1649–1656, 1613–1617 and 1247–1250 cm^{-1}, respectively, affording a shift in their position in the ligand spectrum by 19–26, 5–9 and 35–38 cm^{-1} which are large enough to confirm the involvement of C=O, C=N and C–O (phenolic) in ligation to the metal centre. Nearly no shift in the position of secondary alcoholic C–O band and hence no probable involvement of such band in coordination to the metal centre.[42]

In the spectrum of **PANH-Cu** complex, although the band corresponding to ν(C=O) afforded a shift in its position by

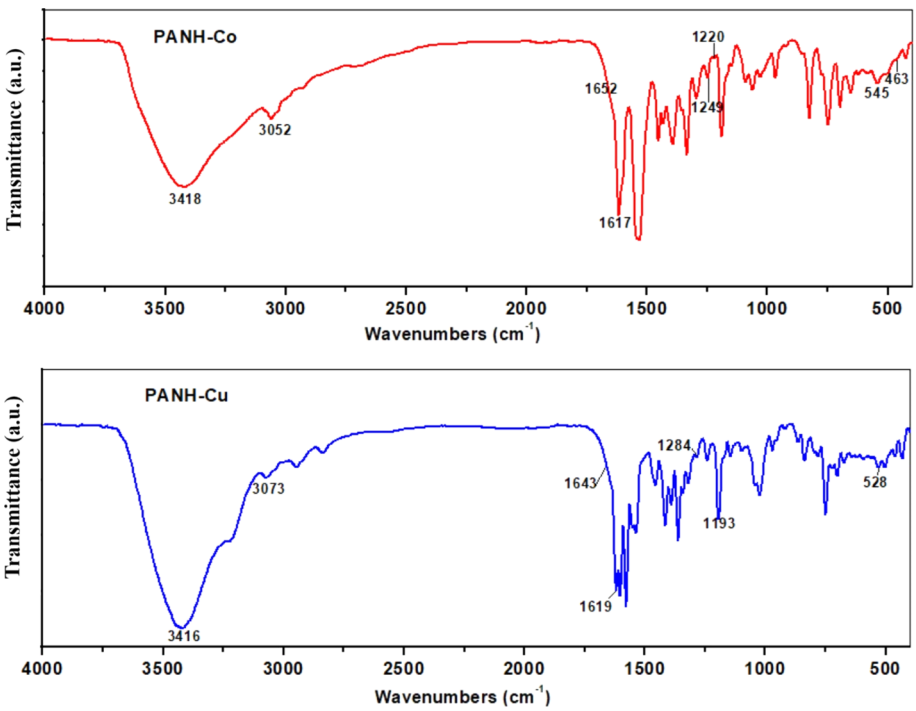

Fig. 5 IR spectra of **PANH-Co** &**PANH-Cu** complexes.

32 cm^{-1} relative to its position in the ligand spectrum, the band corresponding to C=N and C–O (phenolic) bonds appeared almost at the same position relative to the ligand spectrum and hence these two bands are not involved in coordination to the Cu centre. On the other hand, the secondary alcoholic C–O band that appeared in ligand spectrum at 1221 cm^{-1} underwent a shift in its position appearing at 1193 cm^{-1} in **PANH-Cu** complex's spectrum confirming its involvement in ligation to Cu centre through proton removal. The appearance of new bands within the ranges 443–463 cm^{-1} (ν_{M-N}) and 528–545 cm^{-1} (ν_{M-O}) confirms the participation of azomethine nitrogen and phenolic, carbonyl and/or alcoholic O atoms in formation of the complexes.

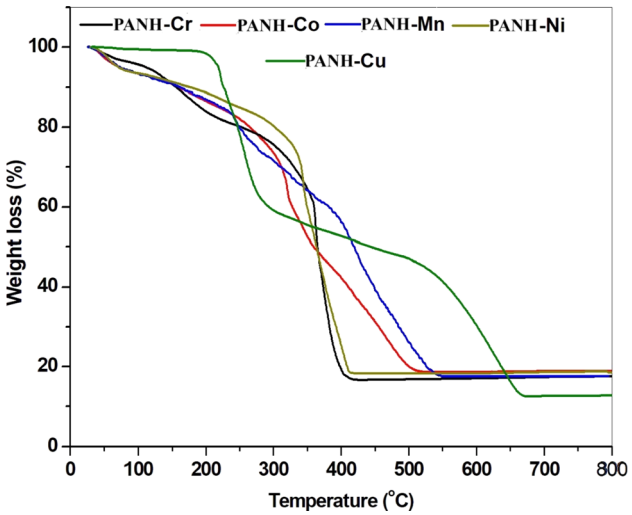

Fig. 6 TGA thermograms of the synthesized metal chelates.

The two non-ligand bands appearing in the spectrum of **PANH-Cr** at 1582 and 1353 cm^{-1} have been assigned to $\nu_{asy}(-COO^{-})$ and $\nu_{sym}(COO^{-})$, respectively, with $\Delta\nu$ separation value of 229 cm^{-1} confirming the coordination of the carboxylate group to the Cr ion in a monodentate fashion.[43]

All complexes' spectra have bands in the ranges 3414–3422 cm^{-1} that are attributed to coordinated and lattice water molecules, whereas the bands in the range 3054–3073 cm^{-1} are attributed to (NH). Although the NH group is not involved in the formation of complexes, H-bond formation is likely responsible for shifting the position of the NH band in the complexes' spectra relative to the free ligand.[44]

3.5. Thermal gravimetric analytical results and kinetic parameters

One of the most helpful methods for predicting the molecular structure and stability of compounds is thermal analysis, which provides vital information on the thermal properties of

Table 3 Interpretation of TG results of metal chelates under interest

Symbol molecular formula (*M*. wt)	Temp. Range (°C)	Mass loss% Found	Mass loss% Calc.	Assignment
PANH-Cr $[[CrL(AOc)_2H_2O]]\cdot H_2O$	25–91	3.65	3.43	Loss of hydration H_2O
525.45	91–330	25.54	25.88	Loss of coordination H_2O and 2 acetate molecules
	330–430	54.32	53.86	Loss of $(C_{18}H_{15}N_2O_{1.5})$
	>430	16.49	16.75	Formation of 0.5 Cr_2O_3 + 1C as residue
PANH-Mn $[MnL(H_2O)_3]\cdot Cl\cdot 2H_2O$	26–105	7.13	7.20	Loss of 2 hydration H_2O
499.80	105–255	13.85	14.20	Loss of 3 coordination H_2O and OH group
	255–399	22.66	22.51	Loss of Cl^{-} anion and dissociation of the organic ligand (C_6H_5)
	399–568	38.60	39.41	Further dissociation of the organic ligand $(C_{12}H_9N_2O)$
	>568	17.76	16.60	Formation of MnO + 1C as residue
PANH-Co $[CoLCl(H_2O)_2]\cdot 3H_2O$	29–113	7.11	7.41	Loss of 2 hydration H_2O
485.78	113–324	30.00	30.57	Loss of coordination H_2O, Cl^{-} anion and C_6H_5.
	324–535	43.42	44.05	Further dissociation of the organic ligand $(C_{12}H_{10}N_2O_2)$
	>535	19.07	17.89	Formation of CoO + 1C as residue
PANH-Ni $[NiL(H_2O)_3]\cdot Cl\cdot 2H_2O$	29–107	7.01	7.15	Loss of 2 hydration H_2O
503.56	107–341	21.44	21.15	Loss of 3 coordination H_2O, Cl^{-} anion and OH group
	341–426	52.37	52.03	Decomposition of the organic ligand $(C_{17}H_{14}N_2O)$ formation of NiO + 2C as residue
	>426	19.18	19.62	
PANH-Cu $[Cu(L)_2]$ 702.21	29–184	—	—	Thermal stability
	184–298	40.70	40.77	Degradation of the ligand moiety and loss of $(C_{20}H_{14}O_2)$
	298–483	11.69	11.97	Loss of $(C_2H_4N_4)$
	483–678	35.72	35.92	Loss of $(C_{16}H_{12}O_3)$
	>678	11.89	11.33	Formation of CuO as residue

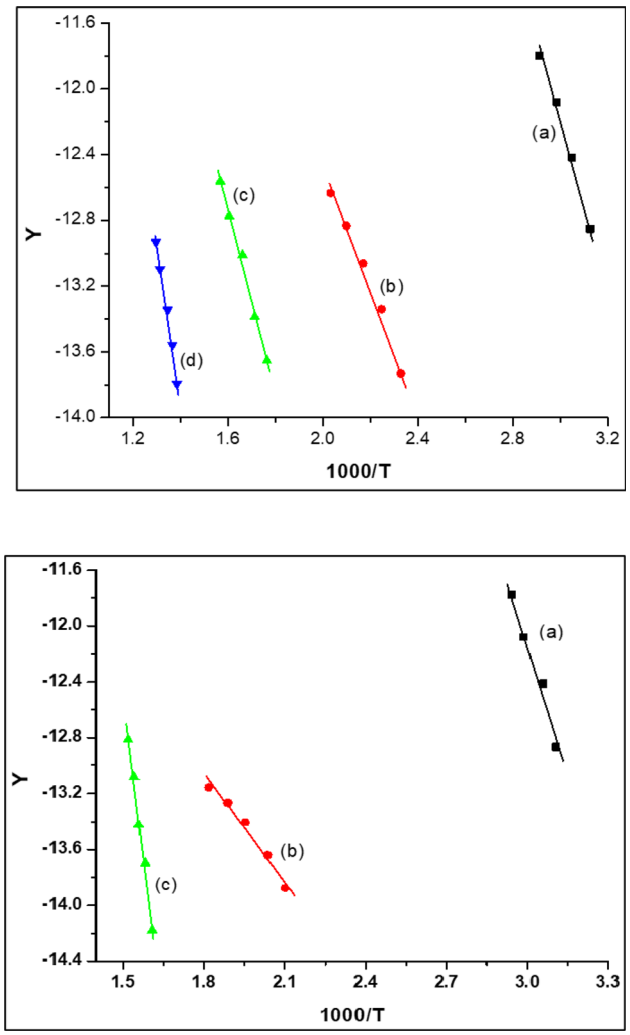

Fig. 7 Coats–Redfern plot for **PANH-Mn** (up) and **PANH-Ni** (down). (a) first step (b) second step (c) third step where, $Y = [-\ln(1-\alpha)]/T^2$ for $n = 1$.

compounds, the phases of thermal degradation, the kinds of intermediates, and the residual products of thermal degradation. Through such examination, the amount and kind of water and/or organic solvent molecules, as well as the other anions attached to the metal center, can be allocated. Thermogravimetric thermograms of the metal complexes are given in Fig. 6 and their analysis are given in details in Table 3. Investigation of the obtained results featured that **PANH-Cr**, **PANH-Co**, **PANH-Ni** and **PANH-Cu** complexes afforded 3-stages thermograms whereas **PANH-Mn** complex has 4-stages thermogram. Analysis of these thermograms showed that, except **PANH-Cu** complex, all the studied compounds started their decomposition from room temperature and the first decomposition stage extended up to 113 °C in which lattice water molecules included in complexes' structures got lost. The following decomposition step started at 91 °C and ended at 341 °C inside which the coordinated water and anion molecules (chloride or acetate) are lost. The successive 1 or 2 stages which started 255 °C and extended to 800 °C are analysed to degradation of the organic ligand molecule incorporated in the complexes' structure and lead to the formation of metallic oxide in addition to small percent of remaining carbon content. For **PANH-Cu** complex with 3-stages thermogram, this complex exhibited thermal stability up to 184 °C and the first stage of decomposition occurred in the range 184–298 °C within which the organic ligand partially decomposed with the loss of 2 molecules of hydroxy naphthyl groups. The second and third stages of decomposition occurred in 298–483 °C and 483–678 °C range and assigned to the loss of $C_2H_4N_4$ and $C_{16}H_{12}O_3$ fragments, respectively, leading to the formation of CuO residue with percent of 11.89% which is in accordance the calculated percent that is 11.33%.

Application of Coats–Redfern equations for the successive decomposition stages enables the computation of the kinetic parameters "order of reaction (n), pre-exponential factor (A), and energy of activation (E)"[45] which have been obtained from

Table 4 Temperature of decomposition and activation parameters (ΔH^*, ΔS^*, ΔG^*) for decomposition of complexes using Coats–Redfern equations

Complex	n	Step	r	T (K)	E_a^*	ΔH^*	A	$-\Delta S^*$	ΔG^*
PANH-Cr	1	1st	0.96834	327.25	65.904	63.6355	0.358 840 874	0.2640	149.95
	1	2nd	0.99910	440	27.254	23.5305	10 392 423.9	0.1222	77.34
	1	3rd	0.98761	647.2	194.344	188.946	2.30388 × 10−5	0.3484	414.47
PANH-Mn	1	1st	0.99581	331.625	41.269	38.5123	3365.103 219	0.1865	100.38
	1	2nd	0.99512	460.8	30.451	26.6200	6 337 456.085	0.1266	84.97
	1	3rd	0.99669	602.8	46.489	41.4031	2 461 953.223	0.1368	125.11
	1	4th	0.99617	745.8	79.119	72.8698	169 515.6068	0.1608	193.75
PANH-Co	1	1st	0.99352	329.125	40.103	37.3675	4752.113 441	0.1836	97.81
	1	2nd	0.98847	469.7	23.166	19.1924	75 716 377.5	0.1063	70.01
	0.5	3rd	0.99849	705	34.466	28.5238	76 813 121.51	0.1095	106.81
PANH-Ni	1	1st	0.98937	331	52.182	49.4307	78.27 469 713	0.2178	121.53
	1	2nd	0.98788	511.7	21.0727	16.7442	124 782 239.6	0.1028	70.29
	1	3rd	0.99575	640.5	128.334	122.970	3.584 854 628	0.2490	283.62
PANH-Cu	—	1st	—	—	—	—	—	—	—
	0.66	2nd	0.99266	529.9	73.858	69.4294	1507.203 925	0.1972	174.49
	0.66	3rd	0.99829	693.6	31.448	25.5912	138 476 513.3	0.1045	99.22
	1	4th	0.99763	894.1	152.693	145.201	183.5 464 653	0.2190	342.62

the plots as shown in Fig. 7 and S6–S8† (Coats–Redfern plot for **PANH-Mn** and **PANH-Ni** complex, as illustrative examples) and the results are depicted in Table 4. The thermodynamic parameters, ΔH, ΔS, and ΔG, were also calculated applying the previous reported equations:

$$\Delta H = \Delta E - RT$$

$$\Delta S = R\left[\ln\frac{Ah}{kT} - 1\right]$$

$$\Delta G = \Delta H - T\Delta S$$

h: Planck constant; k: Boltzmann constant.

Table 4 findings demonstrate the −ve ΔS^* implication that either the activated complex is more ordered than its reactants or that the complexes' normal breakdown process is taking longer than usual.[46] Positive ΔH values signify endothermic breakdown processes.[47] Additionally, it has been found that the vast majority of the time, the heat decomposition stages of all complexes follow zero- or first-order kinetics.

3.6. UV-vis spectra and magnetic moment

DMSO solutions of **PANH** and its metal chelates were synthesized for recording UV-vis spectra which done in the range of 200–800 nm (Fig. S9 & S10†). The free ligand **PANH** showed the absorption band at 276 nm that assigned to $\pi \rightarrow \pi^*$ of C=N group. The bands that appeared at and 310 and 428 nm assigned to $n \rightarrow \pi^*$ transitions of C=N and C=O groups, successively.[43,48] The appearance of such bands in complexes' spectra shifted from these values is evidence for the attachment of both azomethine nitrogen and carbonyl oxygen to the metal ion in complex formation.

For **PANH-Cr** complex, the three observed bands centred at 390, 431 and 523 nm allocated to $^4A_{2g} \rightarrow {}^4T_{1g}$ (P) (ν_3), $^4A_{2g} \rightarrow {}^4T_{1g}$ (F) (ν_2), and $^4A_{2g} \rightarrow {}^4T_{2g}$ (F) (ν_1) transitions, respectively, and confirmed octahedral architecture of the complex.[49,50] The room temperature magnetic moment value of this complex was calculated and found to be of the complex was measured to be 3.82 B. M. that is approaching to the spin only value of three unpaired electrons (*i.e.* 3.88 B. M.) in octahedral Cr(III) chelates and hence confirming the predicted geometry.[50]

In the spectrum of **PANH-Mn** chelate, the three transitions appeared in the spectrum at 586, 464 and 433 nm, respectively, were assigned to $^6A_{1g} \rightarrow {}^4T_{1g}(G)$, $^6A_{1g} \rightarrow {}^4T_{2g}(G)$ and $^6A_{1g} \rightarrow {}^4E_g(G)$ reported for Mn(II) chelates.[51,52] Magnetic moment value of 6.12 B. M. was calculated for this complex which assigned to high spin Mn(II) chelates.

The Co(II) chelate, **PANH-Co**, afforded its spectral bands at 572 and 475 nm that correspond to the transitions $^4T_{1g}(F) \rightarrow {}^4A_{2g}(F)$ and $^4T_{1g}(F) \rightarrow {}^4T_{1g}(p)$, successively, familiar to octahedral Co(II) complexes.[52] Octahedral geometry for this complex is further supported by the magnetic moment value which calculated to be 4.63 B. M.

Octahedral arrangement around the Ni(II) centre in **PANH-Ni** complex was concluded by the appearance of the spectral peaks centred at 520 and 438 nm that attributed to the transitions of

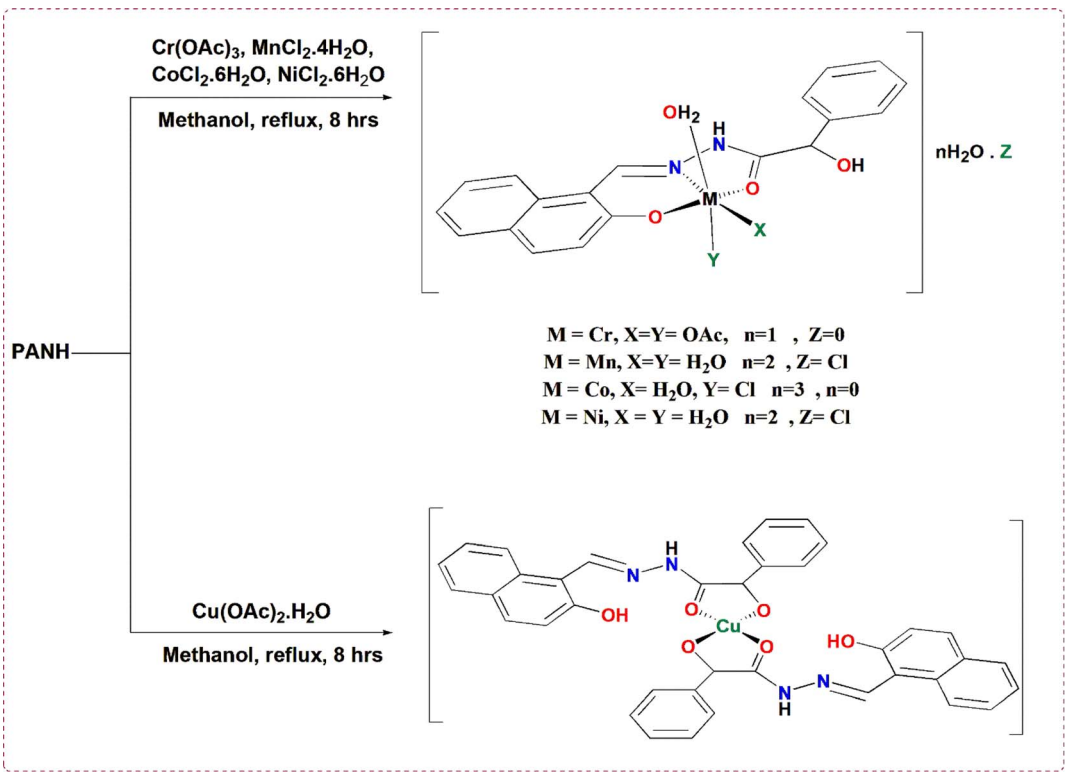

Scheme 1 The structures prospected for the interested metal chelates.

the type $^3A_{2g}(F) \rightarrow {}^3T_{1g}(F)$ (ν_3) and $^3A_{2g}(F) \rightarrow {}^3T_{1g}(P)$ (ν_2) specified for octahedral Ni(II) complexes.[53] Magnetic moment value of 3.32 B. M. was found to **PANH-Ni** complex.

The spectrum of **PANH-Cu** complex represented a broad low-intensity absorption band cantered at 728 nm that assigned to the transition of the type $^2B_{1g} \rightarrow {}^2A_{1g}$ reported for square planar Cu(II) complexes in addition to the peak appearing to 417 nm characteristic for LMCT.[54] Magnetic moment value of 1.84 B. M. was observed for this complex.

Collection of the results obtained above led to the prospected complexes' structures shown in Scheme 1.

3.7. Phenoxazinone synthase effectiveness and kinetic investigation

The existence of the metal complexes interested in this study in a solution containing OAP (*o*-aminophenol) led to its oxidation and generation of APX (2-aminophenoxazine-3-one). Such behaviour was assured by the generation and then increase in the absorbance of APX peak with time. Such band emerged in complexes' spectra at 430, 435, 433 and 428 nm for **PANH-Mn**, **PANH-Co**, **PANH-Ni** and **PANH-Cu** complexes, successively. Thus, the appearance of such band is evidence for the complexes phenoxazinone synthase catalytic efficacy. For **PANH-Cr**, the growing up of such band was not observed with time ensuring that it is not active as a catalyst for such catalytic reaction. The time-dependent spectra of complexes **PANH-Mn**, **PANH-Co**, **PANH-Ni** and **PANH-Cu** with complexes concentration of 3×10^{-5} M and 10^{-2} M concentration of OAP in DMF medium and aerobic conditions are given in Fig. 8–10. For these experiments, time began when OAP was added to the complexes' solutions, and the compounds' spectra were taken every five minutes up to seventy minutes after that. There was no peak observed for (blank experiment). The observed rate constant (k_{obs}) and the initial rate of response (V_o) were determined by using the initial rate method upon using $\varepsilon_{(APX)}$ equals 18 300 M^{-1} cm^{-1}[55] (Table 5).

Kinetics studies were implemented in order to investigate the extent of activity of the metal chelates under study with respect to each other and with respect to reported compounds. This study was done using a concentration of 3×10^{-5} M of the catalyst. To this concentration of the catalyst, alternative substrate concentrations in the range of $(1–8) \times 10^{-3}$ M were separately added. The generates mixtures were subjected to UV-vis spectral recording once the catalyst and the substrate were mixed and after each 3 minutes until the time reached 21 minutes. The absorbances of the generated APX were recorded to calculate the initial rate for the catalytic mixtures. Saturation kinetics were deduced from the shape of the plot of substrate concentrations ([S]) against initial rate (V_o) as obvious in Fig. 11 & 12 demonstrating the pre-equilibrium formation of the complex-substrate intermediate. The rate-determining stage for the catalytic cycle is the irreversible substrate oxidation that developed APX as the product. Such mechanism is well described by the equation:

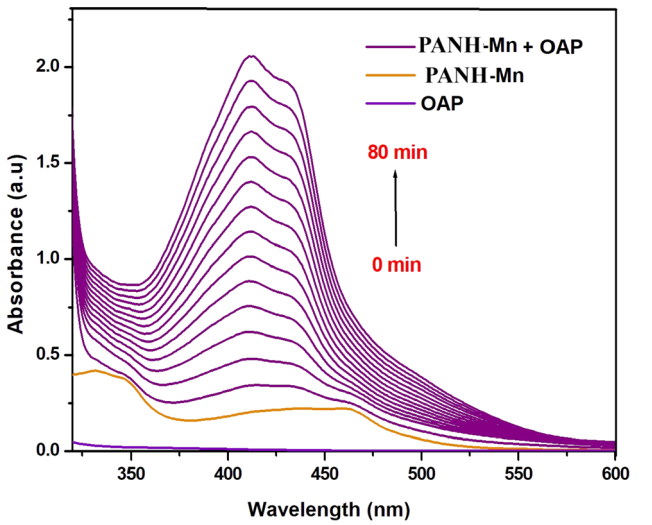

Fig. 8 Variation of UV-vis spectra of **PANH-Mn** chelate with time illustrating the increase of APX peak at 430 nm. The measurement solution contains 10^{-2} M of OAP and 3×10^{-5} M of **PANH-Mn** chelate; DMF is the solvent and aerobic condition.

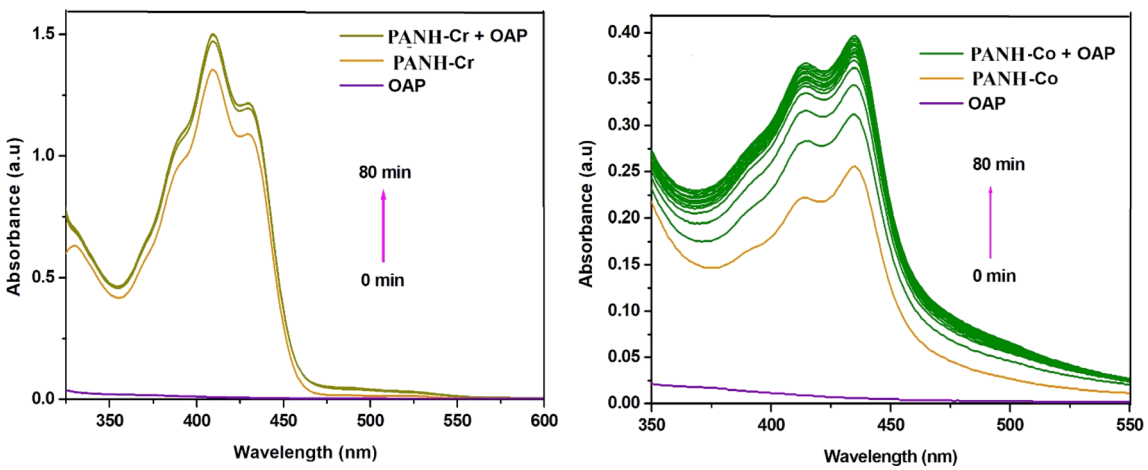

Fig. 9 Variation of UV-vis spectra of **PANH-Cr** and **PANH-Co** chelates with time illustrating the increase of APX peak at 435 nm. The measurement solution contains 10^{-2} M of OAP and 3×10^{-5} M of **PANH-Cr** and **PANH-Co** chelates; DMF is the solvent and aerobic condition.

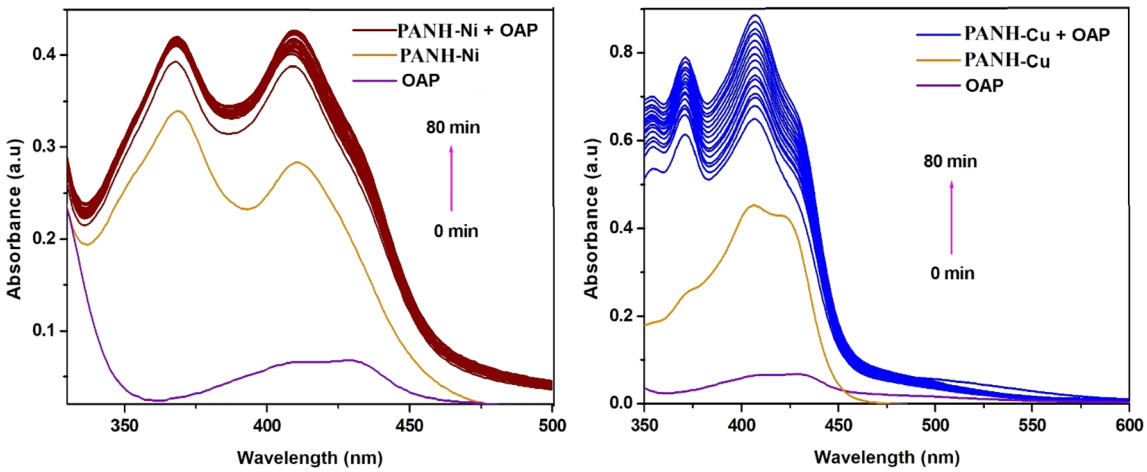

Fig. 10 Variation of UV-vis spectra of **PANH-Ni** and **PANH-Cu** chelates with time illustrating the increase of APX peak at 433, 428 nm, respectively. The measurement solution contains 10^{-2} M of OAP and 3×10^{-5} M of **PANH-Ni** and **PANH-Cu** chelates; DMF is the solvent and aerobic condition.

Table 5 Kinetic parameters for phenoxazine synthase-like activity of the metal complexes under interest

Comp. code	K_{obs} (min^{-1})	V (M min^{-1})	V_{max} (M min^{-1})	K_M (M)	k_{cat} (h^{-1})
PANH-Mn	0.02401	1.31×10^{-6}	8.49×10^{-5}	0.0754	169.89
PANH-Co	0.0038	2.07×10^{-7}	4.74×10^{-7}	1.31×10^{-2}	0.948
PANH-Ni	4.241×10^{-4}	2.32×10^{-8}	2.398×10^{-8}	6.73×10^{-4}	0.048
PANH-Cu	0.0066	3.61×10^{-7}	4.461×10^{-7}	2.704×10^{-3}	0.892

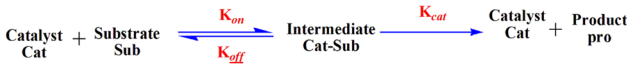

Since the tested catalysts led to saturation kinetics, so, the most suitable equation for treating these reactions is the Michaelis–Menten equation.[34] Application of this equation lead to the calculation of the kinetic parameters V_{max}, K_M and the turnover number (k_{cat}, h^{-1}); Table 5.

Comparison of the results collected in Table 5 demonstrated that the Mn(II) complex **PANH-Mn** exhibited dramatically high activity in comparison with the rest of examined complexes.

Comparison of the activity of the applied complexes based on the obtained results demonstrated that **PANH-Cr** chelate did not show any activity for catalytic the interested reaction (*i.e.* oxidation dimerization of OAP). On the other hand, **PANH-Mn** complex afforded dramatically high activity in comparison with

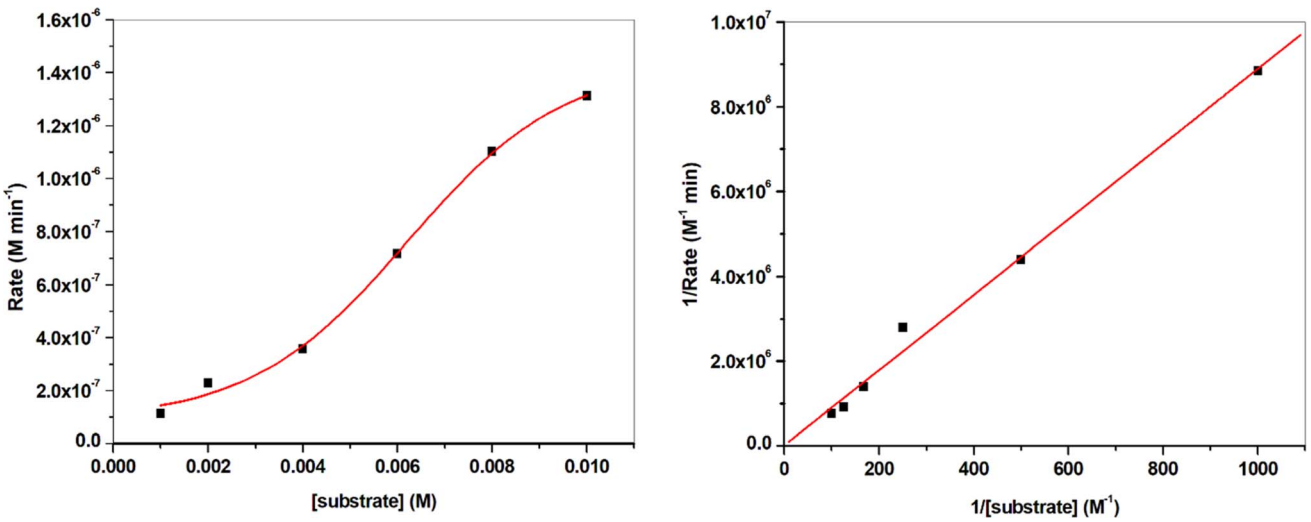

Fig. 11 Plots of Michaelis–Menten (left) and Lineweaver–Burk (right) of **PANH-Mn**.

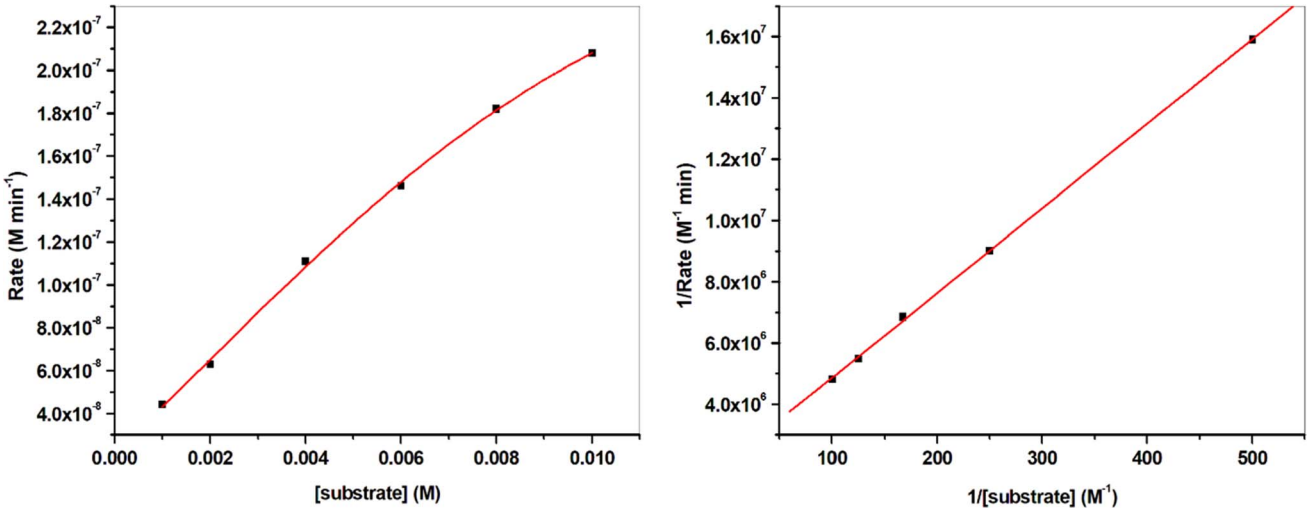

Fig. 12 Plots of Michaelis–Menten (left) and Lineweaver–Burk (right) of PANH-Co.

the rest of examined complexes as observed form its k_{cat} value of 169.89 h^{-1}. The other investigated complexes afforded relatively low activity with k_{cat} in the range 0.048–0.948 h^{-1}.

It is noted that for APX to be produced by the oxidation of OAP by the catalytic action of metal complexes, molecular dioxygen must be present because there almost ever arises a peak of APX in a similar pattern of behavior in the published work.[56,57] So, the prospected mechanism is shown in Scheme 2, taking the structure of the most efficient **PANH-Mn** complex as a model.[28]

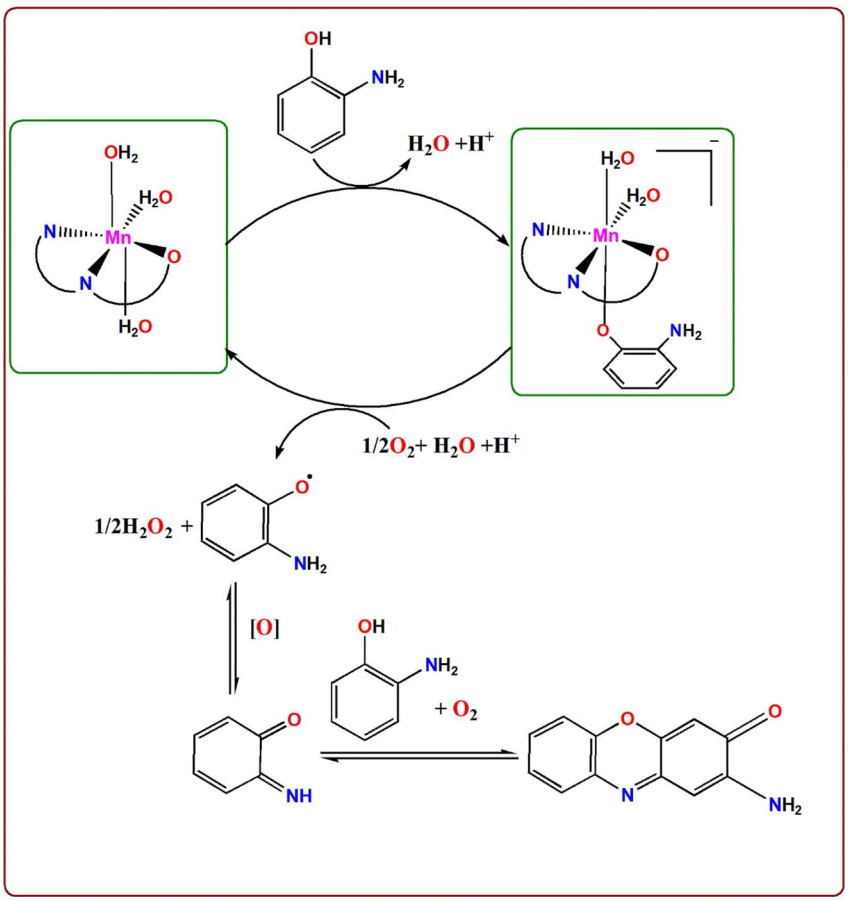

Scheme 2 proposed route for the conversion of OAP to APX by oxidative dimerization catalysed by PANH-Mn.

Since all the investigated complexes are formed with the same ligand, so the key factors affecting their activity are related to the metal centres incorporated in the complexes' structure, their type and oxidation state. Likening the efficacy of the complexes with respect to each other revealed that Cr(III) complex afforded no activity toward oxidation of OAP while the highest activity was exhibited by Mn(II) chelate. For the rest of complexes, the order of activity was **PANH-Co** > **PANH-Cu** > **PANH-Ni**. Precise realization of the complexes' structures also led to notice that all the active complexes contained chloro ligand in their structure while the inactive chromium complex contained acetate ligand in its coordination sphere leading to conclude that the coordinated anion type is also among the factors with dominant the catalysts' efficiency. This behavior can be explained by the accessibility of the first coordination sphere's labile sites, which is preferable for chloro anion over acetate group.[34] Also, the steric influence caused by the CH_3COO^- group's bulkiness relative to Cl^- affect the complexes' reactivity.

4. Conclusion

The trivalent Cr and the divalent Mn, Co, Ni and Cu chelates of the designed Schiff base ligand hydroxy-phenyl-acetic acid (2-hydroxy-naphthalen-1-ylmethylene)-hydrazide have been synthesized and investigated. Successful structure confirmation of the ligand and its metal chelates was achieved by the aid of ^{1}H-NMR, molar conductivity, FTIR, mass, UV-vis spectra, elemental analysis and magnetic moment in addition to analytical results. The empirical formulas of the target metal complexes have been assured to be: $[Cr(PANH)(AOc)_2H_2O]\cdot H_2O$, $[Mn(PANH)(H_2O)_3]\cdot Cl\cdot 2H_2O$, $[Co(PANH)Cl(H_2O)_2]\cdot 3H_2O$, $[Ni(PANH)(H_2O)_3]\cdot Cl\cdot 2H_2O$ and $[Cu(PANH)]$ in which the complexes **PANH-Cr**, **PANH-Mn**, **PANH-Co**, **PANH-Ni** have been formed with the molar ratio 1 L : 1 M whereas **PANH-Cu** complex was formed in the ratio 2 L : 1 M. Molar conductivity values showed that all the complexes have non-electrolytic nature except **PANH-Mn** and **PANH-Ni** complexes are 1 : 1 electrolyte. From the results of FTIR spectra, the ligand has been confirmed to act as monobasic bidentate in **PANH-Cu** complex and monobasic tridentate in the structure of the rest complexes. Octahedral geometry was confirmed to all the complexes except **PANH-Cu** complex which assured to has square planar geometry as concluded from UV-vis spectral results and magnetic moment. The complexes were applied to estimate their activity in oxidation coupling of *o*-aminophenol (OAP) to 2-aminophenoxazine-3-one (APX) revealing an extremely high activity for the Mn(II) complex **PANH-Mn** with k_{cat} value of 169.89 h^{-1}. The other complexes afforded low efficiency with TOF numbers within 0.048–0.948 h^{-1} range while **PANH-Cr** complex afforded no catalytic activity. The other examined complexes afforded relatively low activity in comparison to Mn(II) complex. The uneven catalytic behavior of the metal complex can be explained on the basis of different metal center included in the complexes' structure (*i.e.*, Cr, Mn, Co, Ni and Cu), different oxidation states of metal centers (*i.e.* +2 or +3) and the different surrounding environments concerned with different coordinating anions (*i.e.* chloro or acetate).

Conflicts of interest

There are no conflicts to declare.

References

1 M. M. E. Shakdofa, M. H. Shtaiwi and N. Morsy, Metal complexes of hydrazones and their biological, analytical and catalytic applications: A review, *Main Group Chem.*, 2014, **13**, 187–218.
2 Y. S. Moroz, K. Kulon, M. Haukka, E. Gumienna-Kontecka, H. Kozłowski, F. Meyer and I. O. Fritsky, Synthesis and structure of [2 x 2] molecular grid copper(II) and nickel(II) complexes with a new polydentate oxime-containing Schiff base ligand, *Inorg. Chem.*, 2008, **47**, 5656–5665.
3 M. D. K. Hossain, M. O. Plutenko, J. A. Schachner, M. Haukka, N. C. Mosch-Zanetti, I. O. Fritsky and E. Nordlander, Dioxomolybdenum(VI) complexes of hydrazone phenolate ligands - syntheses and activities in catalytic oxidation reactions, *J. Indian Chem. Soc.*, 2021, **98**, 100006.
4 B. Oinam Chanu, A. Kumar, A. Ahmed and R. A. Lal, Synthesis and characterisation of heterometallic trinuclear copper(II) and zinc(II) complexes derived from bis(2-hydroxy-1-naphthaldehyde) oxaloyldihydrazone, *J. Mol. Struct.*, 2012, **1007**, 257–274.
5 S. A. Yasrebi, H. Mobasheri, I. Sheikhshoaie and M. Rahban, DNA-binding studies of two dioxomolybdenum(VI) complexes of salicylaldehyde benzoylhydrazone ligands, *Inorg. Chim. Acta*, 2013, **400**, 222–227.
6 A. A. R. Despaigne, F. B. Da Costa, O. E. Piro, E. E. Castellano, S. R. W. Louro and H. Beraldo, Complexation of 2-acetylpyridine- and 2-benzoylpyridine-derived hydrazones to copper(II) as an effective strategy for antimicrobial activity improvement, *Polyhedron*, 2012, **38**(1), 285–290.
7 Q. C. Ton, M. Bolte and E. Egerta, Structural similarities among eight benzoylhydrazones, *Acta Crystallogr.*, 2014, **C70**, 912–919.
8 R. M. Issa, S. A. Abdel-Latif and H. A. Abdel-Salam, Synthesis and characterization of new Cu(II) complexes derived from benzilic and mandelic hydrazones, *Synth. React. Inorg. Met.-Org. Chem.*, 2001, **31**(1), 95–105.
9 M. Padmaja, J. Pragathi and C. G. Kumari, Synthesis, spectral characterization, molecular modeling and biological activity of first row transition metal complexes with Schiff base ligand derived from chromone-3-carbaldehyde and o-amino benzoic acid, *J. Chem. Pharm. Res.*, 2011, **3**, 602–613.
10 K. Kiranmai, Y. Prashanthi and N. Subhashini, Synthesis, characterization and biological activity of metal complexes of 3-amino-5-methyl isoxazole Schiff bases, *J. Chem. Pharm. Res.*, 2010, **2**, 375–384.
11 A. D. M. Mohamad, M. J. A. Abualreish and A. M. Abu-Dief, Antimicrobial and anticancer activities of cobalt (III)-hydrazone complexes: Solubilities and chemical potentials

of transfer in different organic co-solvent-water mixtures, *J. Mol. Liq.*, 2019, **290**, 111162.

12 A. M. Abu-Dief, R. M. El-khatib, S. M. El Sayed, S. Alzahrani, F. Alkhatib, G. El-Sarrag and M. Ismael, Tailoring, structural elucidation, DFT calculation, DNA interaction and pharmaceutical applications of some aryl hydrazone Mn(II), Cu(II) and Fe(III) complexes, *J. Mol. Struct.*, 2021, **1244**, 131017.

13 M. A. Jabeen, Comprehensive Review on Analytical Applications of Hydrazone Derivatives, *J. Turk. Chem. Soc., Sect. A*, 2022, **9**(3), 663–698.

14 M. Bagherzadeh, M. Zare, V. Amani, A. Ellern and L. K. Woob, Dioxo and oxo-peroxo molybdenum(VI) complexes bearing salicylidene 2-picoloyl hydrazone: Structures and catalytic performances, *Polyhedron*, 2013, **53**, 223–229.

15 O. Pouralimardan, A. C. Chamayou, C. Janiak and H. Hosseini-Monfared, Hydrazone Schiff base-manganese(II) complexes: Synthesis, crystal structure and catalytic reactivity, *Inorg. Chim. Acta*, 2007, **360**, 1599–1608.

16 S. Balgotra, P. K. Verma, R. A. Vishwakarma and S. D. Sawant, Catalytic advances in direct functionalizations using arylated hydrazines as the building blocks, *Catal. Rev.*, 2019, **62**, 406–479.

17 W. Xiao, Z. L. Lu, C. Y. Su, K. B. Yu, L. R. Deng, H. Q. Liu and B. S. Kang, Bivalent transition metal complexes of 4,5-diazafluorene-9-one benzoylhydrazone (HL) and the characterization of weak interaction in $CoL_2(H_2O)_2$, *J. Mol. Struct.*, 2000, **553**, 91–99.

18 J. Patole, U. Sandbhor, S. Padhye, D. N. Deobagkar, C. E. Anson and A. Powell, Structural chemistry and In vitro antitubercular activity of acetylpyridine benzoyl hydrazone and its copper complex against Mycobacterium smegmatis, *Bioorg. Med. Chem. Lett.*, 2003, **13**, 51–55.

19 M. Yamamoto, K. Sakurai, A. Eguchi, S. Yamazaki, S. F. Nakayama, T. Isobe, A. Takeuchi, T. Sato, A. Hata, C. Mori and H. Nitta, Association between blood manganese level during pregnancy and birth size: The Japan environment and children's study (JECS), *Environ. Res.*, 2019, **172**, 117–126.

20 S. Vaddypally, S. K. Kondaveeti and M. J. Zdilla, Synthesis of a high-valent, four-coordinate manganese cubane cluster with a pendant Mn atom: photosystem II-inspired manganese–nitrogen clusters, *Inorg. Chem.*, 2012, **51**, 3950–3952.

21 M. M. Najafpour, B. Pashaeia and Z. Zanda, Photodamage of the manganese–calcium oxide: a model for UV-induced photodamage of the water oxidizing complex in photosystem II, *Dalton Trans.*, 2013, **42**, 4772–4776.

22 N. Schuth, Z. Liang, M. Schönborn, A. Kussicke, R. Assunção, I. Zaharieva, Y. Zilliges and H. Dau, Inhibitory and Non-Inhibitory NH3 Binding at the Water-Oxidizing Manganese Complex of Photosystem II Suggests Possible Sites and a Rearrangement Mode of Substrate Water Molecules, *Biochemistry*, 2017, **56**, 6240–6256.

23 S. Vaddypally, S. K. Kondaveeti, J. H. Roudebush, R. J. Cava and M. J. Zdilla, Formation of the tetranuclear, tetrakis-terminal-imido Mn 4 IV (N t Bu) 8 cubane cluster by four-electron reductive elimination of t BuN [double bond, length as m-dash] N t Bu. The role of the s-block ion in stabilization of high-oxidation state intermediates, *Chem. Commun.*, 2014, **50**, 1061–1063.

24 S. Vaddypally, S. K. Kondaveeti, S. Karki, M. M. V. Vliet, R. J. Levis and M. J. Zdilla, Reactive Pendant Mn=O in a Synthetic Structural Model of a Proposed S4 State in the Photosynthetic Oxygen Evolving Complex, *J. Am. Chem. Soc.*, 2017, **139**, 4675–4681.

25 S. Vaddypally, D. J. Jovinelli, I. G. McKendry and M. J. Zdilla, Covalent Metal–Metal-Bonded Mn4 Tetrahedron Inscribed within a Four-Coordinate Manganese Cubane Cluster, As Evidenced by Unexpected Temperature-Independent Diamagnetism, *Inorg. Chem.*, 2017, **56**, 3733–3737.

26 Y. Kim, S. Das, S. Bhattacharya, S. Hong, M. G. Kim, M. Yoon, S. Natarajan and K. Kim, Metal-Ion Metathesis in Metal–Organic Frameworks: A Synthetic Route to New Metal–Organic Frameworks, *Chem.–Eur. J.*, 2012, **18**, 16642–16648.

27 A. Das, M. Chakraborty, S. Maity and A. Ghosh, The catalytic activities and magnetic behaviours of rare μ3-chlorido and μ1,1,1-azido bridged defective dicubane tetranuclear Mn(II) complexes, *Dalton Trans.*, 2019, **48**, 9342–9356.

28 S. Banerjee, P. Brandão, A. Bauzá, A. Frontera, M. Barceló-Oliver, A. Panja and A. Saha, Nuclearity versus oxidation state in the catalytic efficiency of MnII/III azo Schiff base complexes: computational study on supramolecular interactions and phenoxazinone synthase-like activity, *New J. Chem.*, 2017, **41**, 11607–11618.

29 S. Ganguly, P. Kar, M. Chakraborty and A. Ghosh, The First Alternating Mn^{II}-Mn^{III} 1D Chain: Structure, Magnetic Properties and Catalytic Oxidase Activities, *New J. Chem.*, 2018, **42**, 9517–9529.

30 A. Panja, Metal ionic size directed complexation in manganese(II) coordination chemistry: efficient candidates showing phenoxazinone synthase mimicking activity, *RSC Adv.*, 2014, **4**, 37085–37094.

31 S. K. Fathalla, H. A. El-Ghamry and M. Gaber, Ru(III) complexes of triazole based Schiff base and azo dye ligands: An insight into the molecular structure and catalytic role in oxidative dimerization of 2-aminophenol, *Inorg. Chem. Commun.*, 2021, **129**, 108616.

32 A. Panja, M. Shyamal, A. Saha and T. K. Mandal, Methylene bridge regulated geometrical preferences of ligands in cobalt(III) coordination chemistry and phenoxazinone synthase mimicking activity, *Dalton Trans.*, 2014, **43**, 5443–5452.

33 S. Dasgupta, J. Adhikary, S. Giri, A. Bauza, A. Frontera and D. Das, Unveiling the effects of in situ generated arene anion radical and imine radical on catecholase like activity: A DFT supported experimental investigation, *Dalton Trans.*, 2017, **46**, 5888–5900.

34 H. A. El-Ghamry, B. K. Alharbi, K. M. Takroni and A. M. Khedr, A series of nanosized Cu(II) complexes based on sulfonamide azo dye ligands: An insight into complexes molecular structures, antimicrobial, antitumor and

catalytic performance for oxidative dimerization of 2-aminophenol, *Appl. Organomet. Chem.*, 2023, **37**, e6978.

35 A. Panja, Exclusive selectivity of multidentate ligands independent on the oxidation state of cobalt: influence of steric hindrance on dioxygen binding and phenoxazinone synthase activity, *Dalton Trans.*, 2014, **43**, 7760–7770.

36 Y. M. Ahn, L. Vogeti, C.-J. Liu, H. K. R. Santhapuram, J. M. White, V. Vasandani, L. A. Mitscher, G. H. Lushington, P. R. Hanson, P. R. Hanson, D. R. Powell, R. H. Himes, K. F. Roby, Q. Ye and G. I. Georg, Design, synthesis, and antiproliferative and CDK2-cyclin a inhibitory activity of novel flavopiridol analogues, *Bioorg. Med. Chem.*, 2007, **15**, 702–713.

37 T. Akhtar, S. Hameed, K. M. Khan, A. Khan and M. I. Choudhary, Design, synthesis, and urease inhibition studies of some 1,3,4-oxadiazoles and 1,2,4-triazoles derived from mandelic acid, *J. Enzyme Inhib. Med. Chem.*, 2010, **25**(4), 572–576.

38 S. M. Sparks, C.-L. Chen and S. F. Martin, Tandem intramolecular benzyne–furan cycloadditions. Total synthesis of vineomycinone B2 methyl ester, *Tetrahedron*, 2007, **63**, 8619–8635.

39 W. J. Geary, The use of conductivity measurements in organic solvents for the characterisation of coordination compounds, *Coord. Chem. Rev.*, 1971, **7**, 81–122.

40 I. A. Waseem, A. Wani and K. Saleem, Empirical formulae to molecular structures of metal complexes by molar conductance, *Synth. React. Inorg., Met.-Org., Nano-Met. Chem.*, 2013, **43**, 1162–1170.

41 K. Nakamoto, *Infrared Spectra of Inorganic and Coordination Compounds*, Wiley, New York, 1986.

42 H. A. El-ghamry, K. M. Takroni, D. O. AL-Rashidi, E. S. Alfear and R. A. Alsaedi, Design, spectral, thermal decomposition, antimicrobial, docking simulation and DNA binding tendency of sulfisoxazole azo dye derivative and its metal chelates with Mn^{2+}, Fe^{3+}, Co^{2+}, Ni^{2+}, Cu^{2+}, Zn^{2+} and Cd^{2+}, *Appl. Organomet. Chem.*, 2022, **36**, 1.

43 M. Gaber, S. K. Fathalla and H. A. El-Ghamry, 2,4-Dihydroxy-5-[(5-mercapto-1H -1,2,4-triazole-3-yl)diazenyl]benzaldehyde acetato, chloro and nitrato Cu(II) complexes: Synthesis, structural characterization, DNA binding and anticancer and antimicrobial activity, *Appl. Organomet. Chem.*, 2019, **33**, e4707.

44 K. El-Baradie, R. El-Sharkawy, H. El-Ghamry and K. Sakai, Synthesis and characterization of Cu(II), Co(II) and Ni(II) complexes of a number of sulfadrug azodyes and their application for wastewater treatment, *Spectrochim. Acta, Part A*, 2014, **121**, 180–187.

45 A. W. Coats and J. Redfern, Kinetic Parameters from Thermogravimetric Data, *Nature*, 1964, **201**, 68–69.

46 A. A. Frost, R. G. Pearson, *Kinetics and Mechanisms*, Inc., New York, 1961, vol. 19.

47 U. El-Ayaan, I. Kenawy and Y. A. El-Reash, Synthesis, thermal and spectral studies of first-row transition metal complexes with Girard P reagent-based ligand, *Spectrochim. Acta, Part A*, 2007, **68**, 211–219.

48 N. H. Yarkandi, H. A. El-Ghamry and M. Gaber, Synthesis, spectroscopic and DNA binding ability of Co^{II}, Ni^{II}, Cu^{II} and Zn^{II} complexes of Schiff base ligand (E)-1-(((1H-benzo[d]imidazole-2-yl)methylimino)methyl)naphthalen-2-ol. X-ray crystal structure determination of cobalt (II) complex, *Mater. Sci. Eng., C*, 2017, **75**, 1059.

49 G. B. Deacon and R. J. Phillips, Relationships between the carbon-oxygen stretching frequencies of carboxylato complexes and the type of carboxylate coordination, *Coord. Chem. Rev.*, 1980, **33**, 227–250.

50 M. S. Refata, T. Altalhia, S. B. Bakareb, G. H. Al-Hazmic and K. Alam, New Cr(III), Mn(II), Fe(III), Co(II), Ni(II), Zn(II), Cd(II), and Hg(II) Gibberellate Complexes: Synthesis, Structure, and Inhibitory Activity Against COVID-19 Protease, *Russ. J. Gen. Chem.*, 2021, **91**(5), 890–896.

51 F. A. Cotton, G. Wilkinson, C. A. Murillo, M. Bochmann, *Advanced Inorganic Chemistry*, Wiley, New York, 6th edn, 1999.

52 M. Gaber, H. A. El-Ghamry and S. K. Fathalla, Synthesis, structural identification, DNA interaction and biological studies of divalent Mn, Co and Ni chelates of 3-amino-5-mercapto-1,2,4-triazole azo ligand, *Appl. Organomet. Chem.*, 2020, **34**, e5678.

53 A. B. P. Lever, *Inorganic Electronic Spectroscopy*, Elsevier, Amsterdam, 2nd edn, 1984.

54 G. I. Mohammed, H. A. El-Ghamry and A. L. Saber, Rapid, sensitive, and selective copper (II) determination using sensitive chromogenic azo dye based on sulfonamide, *Spectrochim. Acta, Part A*, 2021, **247**, 119103.

55 L. Gasque, A. Mendieta and G. Ferrer-Sueta, Comment on "Mixed azido/phenoxido bridged trinuclear Cu(ii) complexes of Mannich bases: synthesis, structures, magnetic properties and catalytic oxidase activities", *Dalton Trans.*, 2018, **47**, 9385–9399; L. Gasque, A. Mendieta and G. Ferrer-Sueta, Tri- and hexa-nuclear Ni^{II}–Mn^{II} complexes of a N_2O_2 donor unsymmetrical ligand: synthesis, structures, magnetic properties and catalytic oxidase activities, *Dalton Trans.*, 2018, **47**, 13957–13971; *Dalton Trans.*, 2020, **49**, 3365–3368.

56 W. P. Sohtun, S. Muthuramalingam, M. Sankaralingam, M. Velusamy and R. Mayilmurugan, Copper(II) complexes of tripodal ligand scaffold (N_3O) as functional models for phenoxazinone synthase, *J. Inorg. Biochem.*, 2021, **216**, 111313.

57 A. Mandal, A. Sarkar, A. Adhikary, D. Samanta and D. Das, Structure and Synthesis of Copper Based Schiff base and Reduced Schiff base Complex: A Combined Experimental and Theoretical Investigation of Biomimetic Catalytic Activity, *Dalton Trans.*, 2020, **49**, 15461–15472.